Design and Fabrication of an Erectable Truss for Precision Segmented Reflector Application

Harold G. Bush,* Catherine L. Herstrom,† Walter L. Heard Jr.,‡ Timothy J. Collins,§ and W. B. Fichter§
NASA Langley Research Center, Hampton, Virginia 23665
and
Richard E. Wallsom¶ and James E. Phelps**
Lockheed Engineering and Sciences Company, Hampton, Virginia 23666

The design of a first generation, 4-m-diam, doubly curved, tetrahedral support truss for precision parabolic reflector panels, incorporating joints specifically designed for on-orbit astronaut assembly, is presented. Operational and design features of the erectable joint are detailed. Methods used to achieve very accurate strut lengths are described. Initial static and dynamic truss test results are presented that demonstrate linear structural response and predictability. Truss surface accuracy, determined photogrammetrically, is shown to be within 0.003 in. (rms) of design.

Introduction

THE NASA Precision Segmented Reflector (PSR) technology development program is a cooperative effort between the Jet Propulsion Laboratory (JPL) and NASA Langley Research Center (LaRC). One objective of the PSR program is to develop a design, fabrication, and orbital-assembly capability for large-diameter, highly accurate, low-mass, orbiting instruments for both Earth and space observation. These instruments require extremely accurate surfaces to enable their operation at near-optical wavelengths. In Fig. 1, one measure of a reflector's quality, the achievable rms surface accuracy, is shown for several existing reflector concepts. The mesh reflector concepts are shown to have achievable rms surface accuracies in the range of 0.03–0.06 in.[1-3] Continued development is expected to improve flexible surface reflector accuracy; however, the improvement will not be sufficient to meet many anticipated future needs. Higher precision reflectors probably require solid surfaces, such as stiff, doubly curved panels, precisely mounted on a stiff, stable, and accurate foundation. This form of construction, illustrated in Fig. 2, is under development to achieve the accuracy required by various Earth and space observation programs.

The PSR program has the objective of developing technology that will enable the construction of large, accurate reflectors including those required for the Global Change Initiative[4] indicated in Fig. 1. The initial design and construction effort, however, is centered around a test-bed (TB) structure, which is a nominally 4-m-diam, doubly curved tetrahedral truss. The goal for rms surface accuracy of the PSR TB truss structure is

shown in Fig. 1 to be approximately 0.004 in. However, it is also shown that such surface accuracy was nearly achieved with a planar 8-m LaRC robotic assembly truss using conventional tolerances without any surface accuracy goal. Consequently, LaRC adopted more stringent and accurate fabrication methods and a different design approach for the 4-m doubly curved TB truss to improve its structural rms surface accuracy. It is intended that the 4-m doubly curved TB truss not only satisfy the PSR accuracy goal, but demonstrate a marked improvement, possibly to the accuracy required by the
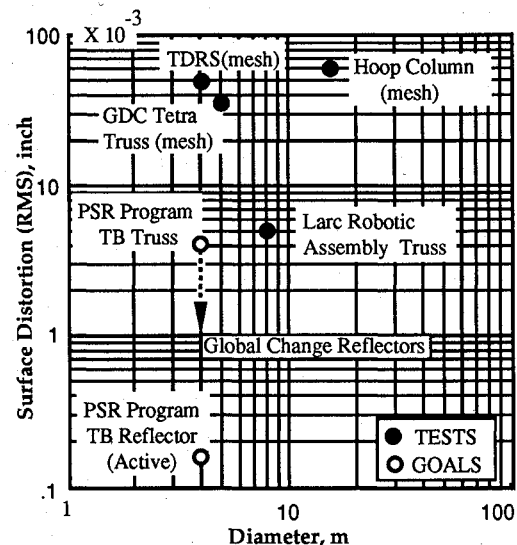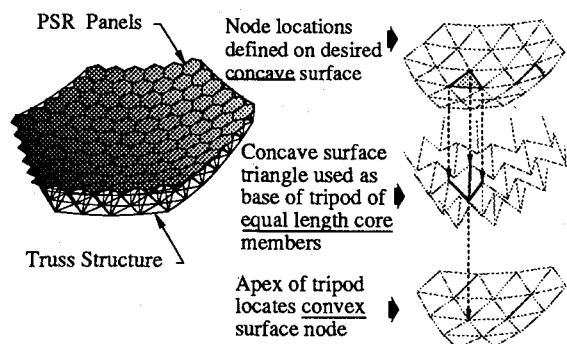

Fig. 1 Reflector surface accuracy.

Fig. 2 Precision segmented reflector geometry.

*Assistant Head, Spacecraft Structures Branch, MS 199. Senior Member AIAA.
†Mathematician, Spacecraft Structures Branch, MS 199.
‡Aerospace Engineer, Spacecraft Structures Branch, MS 199. Senior Member AIAA.
§Aerospace Engineer, Spacecraft Structures Branch, MS 199.
¶Design Engineer, 144 Research Drive. Associate Member AIAA.
**Design Engineer, 144 Research Drive.

Global Change Initiative Reflectors shown in Fig. 1. Achievement of rms surface distortion near 0.0001 in. is expected to require active surface control, as indicated in Fig. 1. However, the active control problem is ameliorated by use of an accurate, stable structure to support the segmented panels and actuators. The TB truss is intended to provide such a foundation for active surface control investigations.

This paper will present design and fabrication features used to build a first generation, erectable precision TB truss structure and to establish its surface accuracy characteristics. Specifically, the objectives for the TB truss were to design and fabricate a doubly curved structure that exhibited 1) a surface deviation of 0.004 in. or less (rms) from design, and 2) linear and predictable structural behavior. Initial structural test results for joints, struts, and the complete truss will be presented and compared with theoretical predictions.

Test-Bed Truss Geometry

The TB truss tetrahedral geometry was designed as shown in Fig. 2. Node locations on the concave surface were prescribed to accommodate reflector panels being developed in other PSR activities (see Ref. 5). The concave surface nodes were connected by various length struts. Three points on the concave surface (see Fig. 2) formed the base of a tripod that had equal length members (core struts). The apex of the tripod defined the nodal location on the truss convex surface. The truss was completed by connecting nodal locations on the convex surface with appropriate length struts. Since core struts comprised approximately one-third of the structure, using equal lengths reduced the fabrication complexity.

A typical tetrahedral node with nine strut joints attached is shown in Fig. 3. Given the global coordinates of the center of each node, a local coordinate system for each node was formed as follows. A line was passed through the apex of each tripod normal to its triangular base plane in the opposite surface to form a local z axis (see Fig. 3). An x axis was located in a plane which contained a surface strut and the z axis. Azimuth angles were defined as the planform (i.e., x-y plane) angle between surface (or core) struts. Elevation angles were defined as the angle between each strut and the z axis. The z axis of each node was used as its rotational machining axis. The doubly curved truss geometry was produced by machining nine facets at the joint intersection locations in the surface of a 2.5-in.-diam spherical node at the correct azimuth and elevation angles (shown in the Fig. 3) relative to the nodal machining axis (z axis). A female cruciform was machined in each facet at the correct rotational angle to insure proper alignment of each nodal joint half. All facets were located (theoretically) at the same spherical radius. Struts of the correct lengths joined nodes to form the desired doubly curved truss. This design method concentrated all unique features of a doubly curved truss into 1) the nodes and 2) different strut lengths. All joint componentry for each strut, which constituted the

greatest part count, was identical. Because of symmetry in the tetrahedral truss chosen, there were three nodes of each design, and at least three struts of each length required, in each surface.

Erectable Joint Features

The TB truss joint was designed to have good structural properties, namely, linear load-displacement behavior and high stiffness, and also to allow easy on-orbit extravehicular activity (EVA) assembly by pressure-suited astronauts. The specific joint design (i.e., 1-in.-diam) evolved from a larger (i.e., 2-in.-diam) joint that was developed for Space Station Freedom application. Features of the larger joint represent developments made in concert with the astronaut corps. It has been the primary joint used in Space Station Freedom assembly studies[6] to date. Because the joint is designed for efficient assembly of the structure, the truss is denoted erectable and the joint is termed an erectable joint. An exploded view of a 1-in.-diam erectable joint and node, detailing construction features, is shown in Fig. 4. Joint node halves (i.e., the half of a joint attached to a node) are attached by an internal turnbuckle stud to the spherical node. The joint halves at the end of each strut have opposite thread directions, permitting the strut to be used as a turnbuckle for accurate length setting during fabrication. The erectable joint is effected by inserting the joint strut half sideways into the joint node half, engaging matching tapered tongues and grooves. A sliding latch bolt permits one-handed capture. Clockwise rotation of the ribbed cam cover operates a rotary cam that further locks and preloads the joint for structural use. Unlocking is accomplished by sliding the cam cover axially away from the node and rotating counterclockwise to withdraw the latch bolt. The joint halves are then free to be disassembled. The female cruciforms, machined into each nodal facet, provide rotational alignment of both joint node halves to which a strut is attached, permitting side insertion of each strut. The side insertion feature permits the assembly of a redundant structure (i.e., inserting a strut between two fixed nodes). All TB truss node and joint components were fabricated from 7075 Al and machined on numerically controlled lathes and/or milling machines for accuracy.

Strut Assembly and Length Setting Method

The TB truss struts were fabricated from graphite epoxy (T300/934) with a ±10-deg filament orientation. The 1-in.-diam tubular struts had a nominal cross-sectional area of 0.1838 in.[2] Threaded aluminum fittings (LH and RH) were bonded into the ends of each strut. Locknuts were used to secure joints to each strut at the prescribed length.

Struts and joints were assembled and set to length using the fixture shown in Fig. 5. Angle plate supports in the fixture replaced nodes in the structure for length setting purposes. Joint node halves were bolted to female cruciforms machined into each angle plate support. One angle plate was bolted to the steel box beam and another angle plate was bolted to a precision air bearing carriage, which also supported a laser interferometer, as shown in the Fig. 5. The angle plate cruciforms aligned both joint node halves in the same direction, so that, when a strut and joint assembly was inserted and locked, the strut could be rotated to set the appropriate length while joint alignment was maintained. The air slide prevented axial preload, which could have affected the length setting. A single reference strut and joint assembly was measured in a coordinate measuring machine (to a tolerance of approximately ±0.0002 in.). This reference strut and joint assembly was installed between the angle plate supports of the fixture and used to establish a zero for the laser interferometer. The radial distance of each nodal facet from the nodal center was also determined using a coordinate measuring machine. These radial distances were appropriately subtracted from the theoretical distance between nodal centers for each strut, yielding a facet-
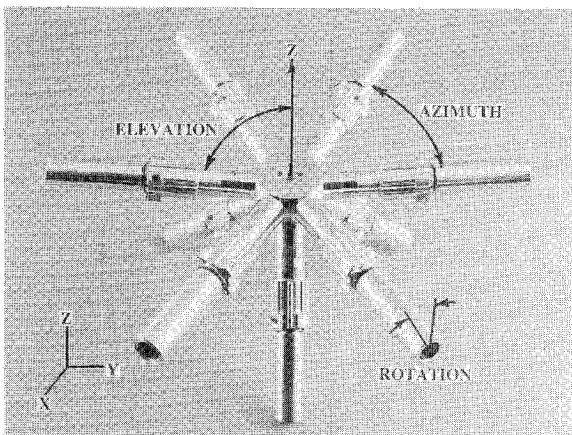

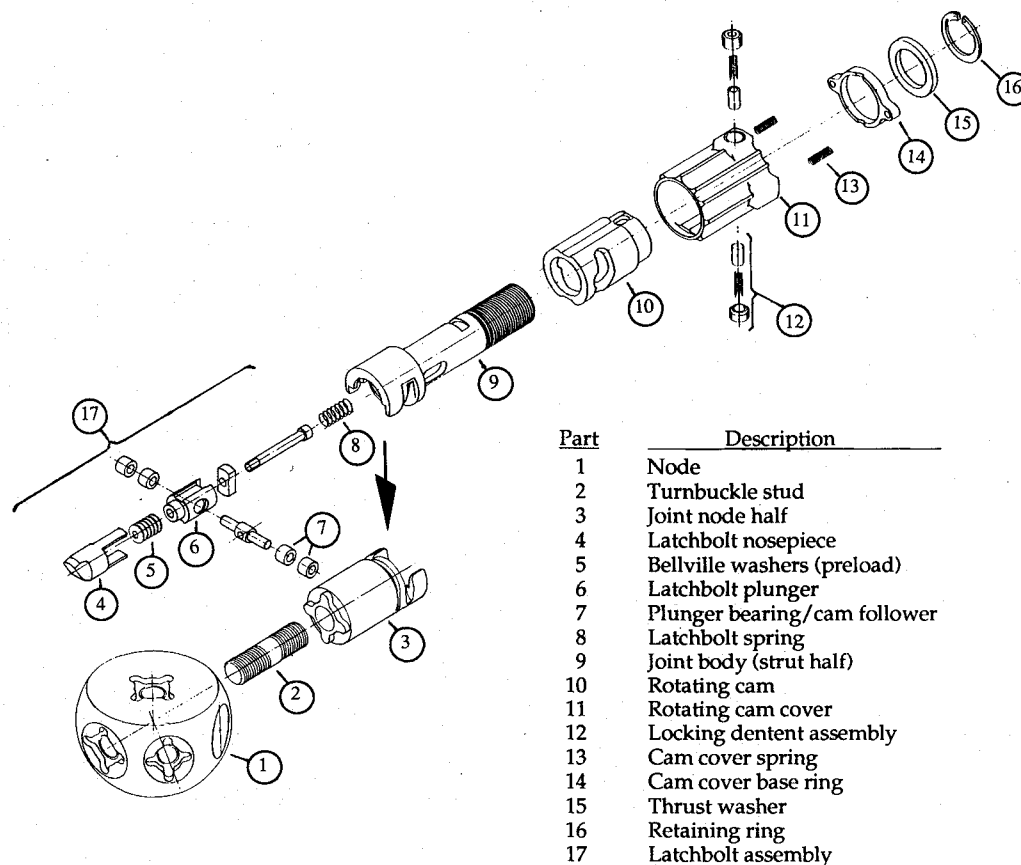Fig. 3 Typical tetrahedral truss node and joint componentry.

Part	Description
1	Node
2	Turnbuckle stud
3	Joint node half
4	Latchbolt nosepiece
5	Bellville washers (preload)
6	Latchbolt plunger
7	Plunger bearing/cam follower
8	Latchbolt spring
9	Joint body (strut half)
10	Rotating cam
11	Rotating cam cover
12	Locking dentent assembly
13	Cam cover spring
14	Cam cover base ring
15	Thrust washer
16	Retaining ring
17	Latchbolt assembly

Fig. 4   Erectable node/joint details—exploded view.
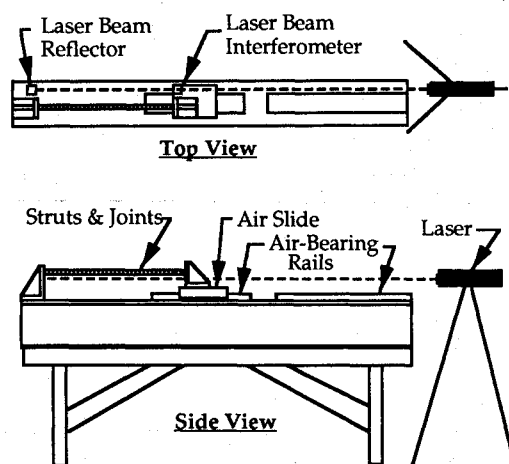
Fig. 5   Strut/joint assembly and length setting fixture with laser interferometer setup.

to-facet strut length. Each strut and joint assembly was set to the theoretically correct facet-to-facet length and locknuts were torqued to prescribed values. Because of the reference strut tolerance (determined by the coordinate measuring machine), the strut lengths had essentially the same tolerance (±0.0002 in.), even though the strut length increments were set to much greater accuracy by use of the laser interferometer. All measurements were made in a temperature controlled environment at 69°F.

Subsequent to assembling and setting the length of all truss struts, three spare struts were subjected to initial and cyclic loads of 50 and ±50×3100 and ±100×3, 150 and ±150×3 lb, respectively. Each strut was remeasured after the initial and cyclic loads. All struts measured after loading varied approximately 0.00005 in. or less from their original length.

Precision Segmental Reflector Test-Bed Truss

The assembled 4-m doubly curved tetrahedral truss is shown in Figs. 6 and 7. The truss, which was designed to accept parabolic panels with a focal length of 2.4 m, consisted of 45 nodes, 150 struts, and 300 joint assemblies and weighed 189 lb. Core strut length between nodal centers was 0.8135 m. After static, dynamic, and photogrammetric characterization, the TB truss will support precision segmented reflector development activities at JPL by providing a robust and accurate foundation for examination of panel attachment and surface control issues.

Joint/Node and Strut Axial Stiffness

Axial stiffness of a joint and node combination was determined by performing a load-displacement test, as shown in Fig. 8. Three direct current differential transformers (DCDT) displacement transformers were located symmetrically around the specimen to measure the distance change between the plates, as shown in the Fig. 8. The transducers had a 0.050-in. range with a potential error of ±0.00025 in. Specimen axial centerline displacement was calculated from the three measurements to eliminate bending effects. Deformations of all connections (threads, tongues, and grooves, etc.) were included in measured displacements. The joint centerline load-displacement response is shown in Fig. 9. The extensional stiffness (modulus × area) for the erectable joint/node assembly (length = 10.31 in.) was found to be 1.9×10^6 lb in the load range of ±300 lb.

Axial stiffness of the graphite/epoxy struts was determined from load-displacement tests using a three DCDT setup similar to that shown in Fig. 8. A typical strut load-displacement response is shown in Fig. 9. The structural response of the strut is shown to be linear with no discernible hysteresis. An average extensional modulus of 16.9×10^6 psi was determined from tests of six struts. The modulus was based on the strut nominal cross-sectional area of 0.1838 in.^{2}, and all results were within 1.5% of the average value.

Joint/Node and Strut Bending Stiffness

A graphite/epoxy strut was tested in bending, as shown in Fig. 10. The effective strut bending stiffness was determined from the load-displacement test results of the simply supported, centrally loaded beam shown in the figure. Bending stiffness (modulus × moment of inertia) of the strut was found to be 2.93×10^5 lb-in.^{2}.

A typical joint was also tested in bending, as shown in Fig. 10. The effective bending stiffness of the joint about the two major axes was determined using the analysis of Ref. 7 in conjunction with the load-displacement results shown in the figure. Bending stiffness (modulus × moment of inertia) was found to be 1.55×10^5 lb-in.^{2} about the major axis and 1.26×10^5 lb-in.^{2} about the minor axis.
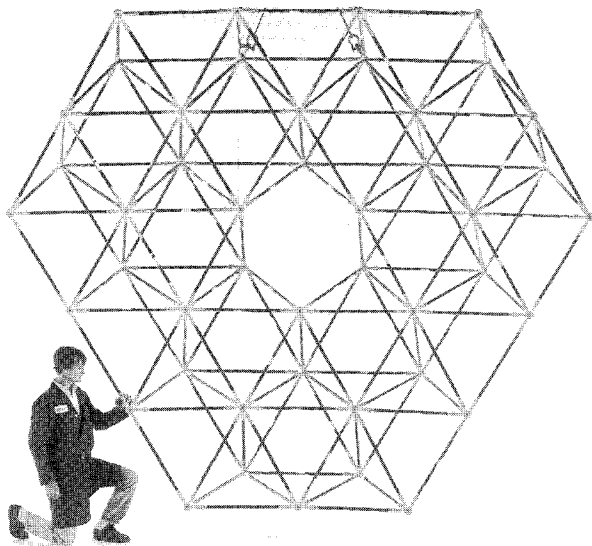
Fig. 6   Erectable 4-m tetrahedral truss test-bed structure (planform view).
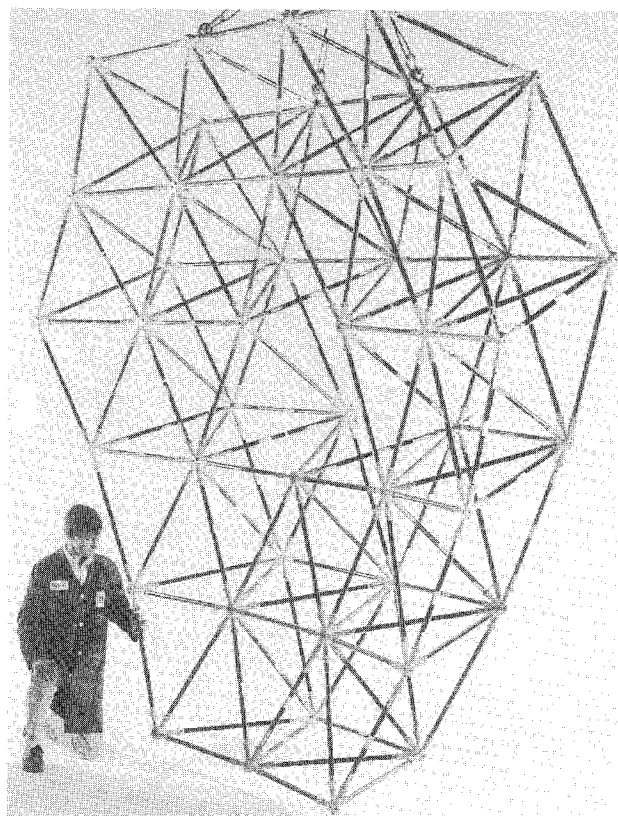
Fig. 7   Erectable 4-m tetrahedral truss test-bed structure (oblique view).
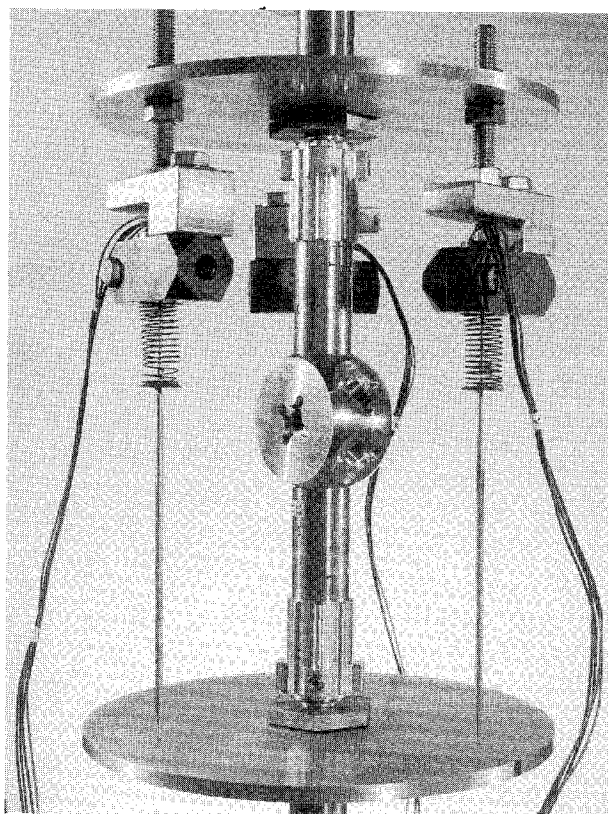
Fig. 8   Erectable node/joint load-displacement test setup.

Truss Analytical Model

Three finite element analysis models of the TB truss were constructed. Results from these analyses are presented to examine differences in modeling complexity (i.e., bending elements vs extensional elements, etc.). Selection of EAL or NASTRAN for the bending element or extensional element models was based solely on the familiarity of the analyst with the codes. A schematic representation of the three analytical models used to represent a strut and joints connecting any two nodes is shown in Fig. 11. Grid points used and element characteristics for MSC/NASTRAN,[8] EAL,[9] and BUNVIS[10] models are noted on the figure. The NASTRAN model used one extensional element to connect two grid points that were located at the truss nodes. Measured strut and joint extensional properties were used to calculate equivalent element extensional properties that were used in the analyses. Strut bending was not included in the NASTRAN model. The EAL model had grid points located at each truss node and three intermediate grid points. One located at the strut center, and one each located at the joint/strut junction. Finite elements with both extensional and bending properties were used to represent the joint/node and tubular section of the complete strut. Measured extensional and bending properties were used in the analyses. The BUNVIS model used grid points located only at the truss nodes, but connected exact beam-column elements representing the joint/node and tubular sections of the strut. This exact substructure element (i.e., strut) connected grid points to model the truss. Measured extensional and bending properties were used in the analyses.

Photogrammetric Survey

For the photogrammetric survey,[11] 0.1-in.-diam reflective targets were centered on the flat surface of all 27 nodes in the truss concave surface. With the photogrammetric camera stationary and elevated, the truss, in the concave-up position, was rotated in 15-deg increments about its vertical axis and photographed obliquely from 24 distinct perspectives. Meas-
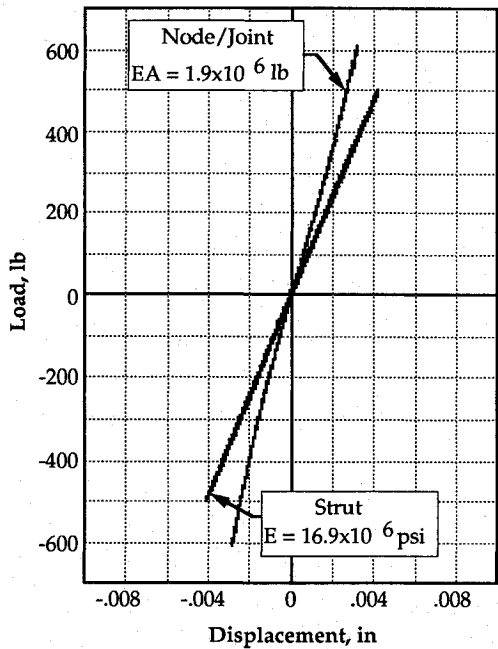
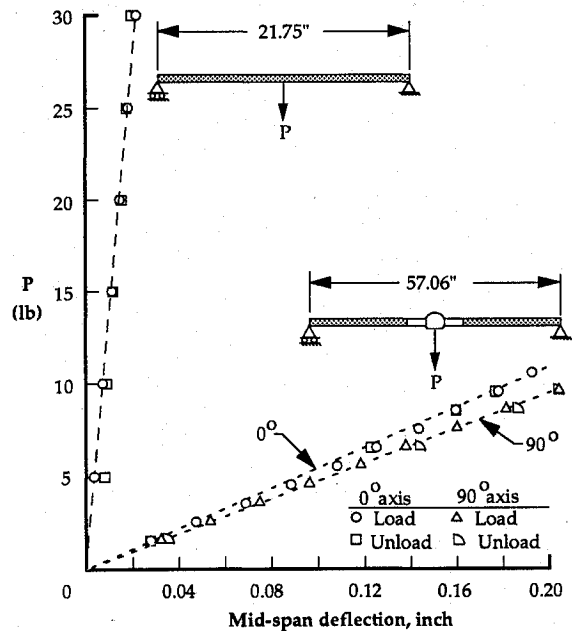Fig. 9   Load-displacement tests of a strut and node/joint assembly.

Fig. 10   Bending load-displacement tests of a strut and a node/joint assembly.

best fit rms difference of 0.00148 in. considering all coordinates. The second assessment used a six-parameter transformation (six rigid-body motions) along with an independently measured 2-m scale, which was present in all the photographs. In this case (see B in Fig. 12), the rms difference was 0.00283 in. considering all coordinates. Also shown in the figure are the rms difference values of each of the x, y, z coordinates. The results for both cases A and B indicate that the rms error in the z coordinate was considerably less sensitive to the analysis procedure than were the rms errors in the x and y coordinates. However, both analyses (i.e., A and B) in Fig. 15 indicate that the PSR goal of 0.004 in. shown in the figure for the TB truss was achieved.

Subsequent to the survey, the displaced target was repositioned and the erroneous node-ball measurement was cor-
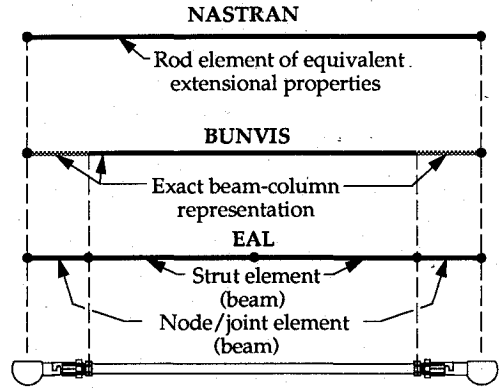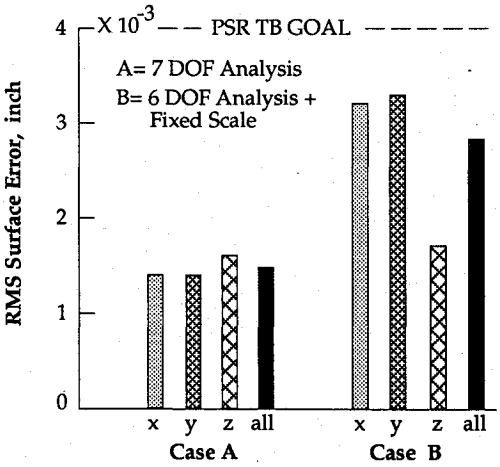

Fig. 11   Truss analytical models.

Fig. 12   Photogrammetric truss surface accuracy.

urements from the photographs, along with target-coordinate predictions from finite element truss analyses, which accounted for gravitational and thermal deformations, were supplied to the photogrammetric analysis program. The combined gravitational and thermal ($\Delta T = 3.6°F$) vertical deflection of the truss concave surface was predicted to be 0.00225 in. or less.

Subsequent to the photogrammetric survey, 2 of the 27 targets were found to be faulty. One target had been inadvertently displaced; the predicted location of the other had been based on an erroneous node-ball measurement. Both targets were omitted from the photogrammetry analyses.

The analysis program was used to produce two assessments of the RMS difference between the predicted and the as-photographed target locations. In producing the first assessment (see A in Fig. 12), the analysis used a seven-parameter transformation (six rigid-body motions and scale) to obtain a
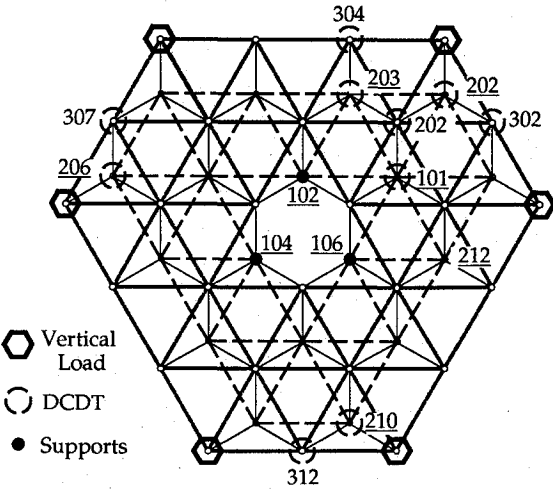

Fig. 13   Static deflection measurement locations.

rected. Upon completion of a longer, more accurate absolute scale that is currently being fabricated, additional photogrammetric surveys are planned.

Truss Static Test

The TB truss was supported vertically on trunnion mounts at nodes 102, 104, and 106 (shown in Fig. 13) of the convex surface on a rigid horizontal bedplate. (Node numbers that are underlined are on the truss convex surface.) Each trunnion mount was bolted to a truss node and was clamped to the bedplate at an offset of 1.65 in. below the node spherical center (i.e., load path). After nonbinding fit up of each mount, trunnion pivots were also clamped. Therefore, support node radial deflection was restrained elastically instead of being fixed. Vertical loads (dead weights) were applied in 20-lb increments through the spherical center of the six corner nodes indicated in Fig. 13. Nodal vertical displacement measurements (DCDTs) were taken at the 10 nodes circled in Fig. 13. Horizontal measurements were also taken at the support node locations, radially toward the truss center. The displacement transducers had a 0.050-in. range with a potential error of ±0.00025 in. Measured vertical deflections at 100-lbf corner load (i.e., six locations) are summarized in Fig. 14 for two tests. The second test reproduced the first so closely that the data points overlap in the figure. Load-displacement response at each point was linear and devoid of discernible hysteresis during unloading. In Fig. 14, the shaded bar at each node location represents the vertical displacement predicted by finite element analysis,[8] which accounted for measured radial displacements of 0.00034, 0.00055, and 0.00048 in., respectively, at support nodes 102, 104, and 106. It is shown in the figure that deviations from predicted deflections varied between 0.0001 and 0.001 in. The greatest deflection prediction errors, about 14% percent, occurred at nodes 203 and 304, which are directly connected vertically by a core strut (see Fig. 13). All other predictions differed from measured deflections by < 8%.

Truss Dynamic Test

The TB truss was tested to determine its dynamic characteristics. Truss frequencies and mode shapes were experimentally obtained for the first 12 modes of the structure. During dynamic testing, the truss support was identical to that used for static testing. Two shakers, attached at nodes 206 and 212 (see Fig. 13), were used simultaneously to excite the truss vibrational frequencies by independently imparting random forces (up to a maximum of 5 lb) to the driving nodes over a frequency range of 0–250 Hz. The frequency response of the structure was measured by triaxial accelerometers placed at each of the 45 truss node locations.

Figure 15 shows two typical frequency response curves for the truss structure that corresponds to accelerometer mea-

surements taken at each driving node location. Each peak indicates a natural frequency of the structure and is well defined. The first 12 truss structural frequencies, determined by analyzing accelerometer data for all of the truss nodes, are identified by marks on the frequency axis. For comparison, initial frequency predictions of the three truss finite element models are also shown in Table 1. Included in the BUNVIS analytical results is the percentage of total strain energy due to strut axial strain in each mode. Each of the three finite element models predicts essentially the same structural frequency for the first seven modes. For modes 8–12, which involve significant strut bending (i.e., axial strain energy < 90%), the EAL and BUNVIS models yield lower, more accurate, frequency predictions than the NASTRAN model, which did not include strut bending effects. Examination of the strain energy shows that modes 11 and 12 (and higher) are largely strut-bending dominated modes, thus, the more detailed EAL and BUNVIS models yield more accurate predictions. Experimental frequencies for all modes (except mode 3) differ from the analytical predictions by approximately 6% or less. Mode 3, an experimental mode at 51.9 Hz, which is not predicted by any of the analyses, is indicated by experimental mode shape results to involve flexibility of the support trunnions. Investigation of this anomaly is continuing. A visual comparison of the first 10 experimental mode shapes, given in Table 1, with the predicted (BUNVIS) mode shape indicates good correlation (except for mode 3).

Concluding Remarks

Design and fabrication features have been described that were employed to produce an accurate truss for supporting precision segmented reflector panels. Joint design details and operational features that permit on-orbit astronaut assembly have been presented. An initial assessment of structural accuracy found the rms surface deviation to be between 0.00148 and 0.00283 in., which meets the PSR test-bed truss objective of 0.004 in. or less. Static test results for the truss and components were found to be linear and repeatable. Comparison of truss static test results with analysis showed the vertical deflection of two directly connected nodes to differ by approximately 14% from prediction. All other predictions were within 8% of measured deflections. Experimental dynamic evaluation of the truss yielded one mode involving elastic boundary conditions, which was not predicted in the initial analyses. All other experimental mode shapes essentially agreed visually with predictions, and frequency agreement was within 1–6%. From the test-bed experimental and analytical results presented herein, it is concluded that this first generation erectable truss demonstrates the validity of the approach for precision segmented reflector application.
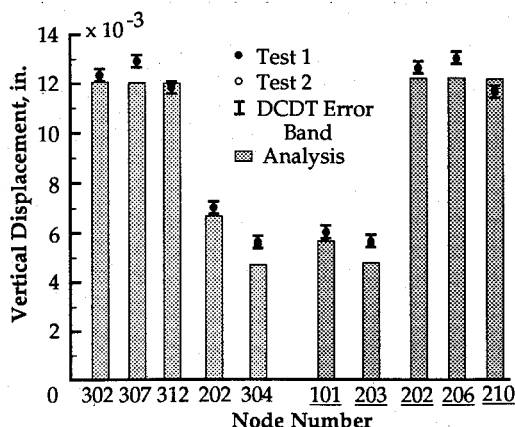

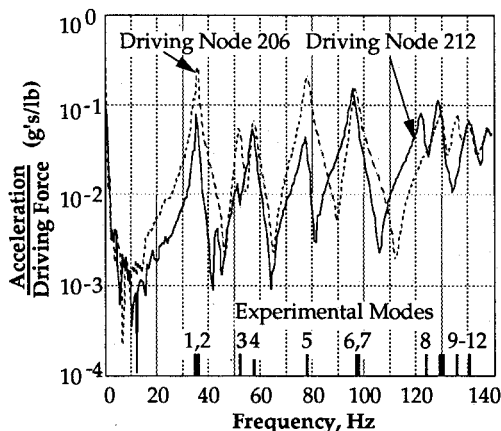Fig. 14   Truss static deflection summary (vertical load = 100 lbf at six locations).
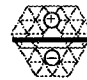
Fig. 15   PSR test-bed frequency response curves (typical).

Table 1   Dynamic results (natural frequencies comparison)

| Analysis | | | | | | | Mode shapes | | | | | |

Mode number	Test	BUNVIS f, Hz	BUNVIS % axial strain energy	EAL f, Hz	NASTRAN f, Hz
1	34.5	35.04	98.4	35.04	34.55
2	35.6	35.05	98.4	35.05	34.55
3	51.9	——	——	——	——
4	57.3	59.73	96.8	59.73	59.54
5	78.1	73.31	91.9	73.32	75.29
6	96.6	92.26	90.0	92.27	93.23
7	97.3	92.33	90.1	92.34	93.23
8	123.7	120.84	74.6	120.86	125.98
9	129.0	125.75	65.4	125.76	143.36
10	130.1	126.90	65.7	126.93	143.36
11	136.0	136.13	0.6	136.21	160.02
12	140.7	137.24	0.3	137.32	177.25

Mode shapes (Mode No. — Test — BUNVIS):

- Mode 1 — Rocking
- Mode 2 — Rocking
- Mode 3 — Rocking + Torsion
- Mode 4 — Torsion
- Mode 5 — Umbrella
- Mode 6 — Saddle
- Mode 7 — Saddle
- Mode 8 — Radial flutes
- Mode 9 — Rocking + Truss Bending
- Mode 10 — Rocking + Truss Bending

References

[1]Campbell, T. G., Bailey, M. C., and Belvin, W. K., "The Development of the 15-Meter Hoop Column Deployable Antenna System with Final Structural and Electromagnetic Performance Results," *Acta Astronautica,* Vol. 17, No. 1, 1988, pp. 69–77.

[2]Kefauver, N., and Cencich, T., "Near Field Testing of the 5-Meter Model of the Tetrahedral Truss Antenna," NASA CR-178147, Aug. 1986.

[3]Bailey, M. C., "Hoop Column and Tetrahedral Truss Electromagnetic Tests," NASA CP-2447, Pt. 2, Nov. 1986, pp. 737–746.

[4]Wright, R. L., and Campbell, T. G. (eds.), "Earth Science Geostationary Platform Technology," NASA CP-3040, July 1989.

[5]Collins, T. J., and Fichter, W. B., "Support Trusses for Large Precision Segmented Reflectors: Preliminary Design and Analysis," NASA TM-101560, March 1989.

[6]Watson, J. J., Heard, W. L., Jr., Bush, H. G., Lake, M. S., Wallsom, R. E., and Phelps, J. E., "Results of EVA/Mobile Transporter Space Station Truss Assembly Tests," NASA TM-100661, Nov. 1988.

[7]Wu, K. C., "Characterization of the Bending Stiffness of Large Space Structure Joints," NASA TM-101565, May 1989.

[8]"MSC/NASTRAN User's Manual," MacNeal-Schwendler Corp., Los Angeles, CA, Rept. MSR-39, Nov. 1985.

[9]Whetstone, W. D., "EISI-EAL Engineering Analysis Language Reference Manual—EISI-EAL System 312," Engineering Information Systems, Inc., San Jose, CA, Aug. 1985.

[10]Anderson, M. S., Williams, F. W., Banerjee, J. R., Durling, B. J., Herstrom, C. L., Kennedy, D., and Warnaar, D. B., "User Manual for BUNVIS-RG: An Exact Buckling and Vibration Program for Lattice Structures, with Repetitive Geometry and Substructuring Options," NASA TM-87669, Nov. 1986.

[11]Brown, D. C., "Application of Close-Range Photogrammetry to Measurements of Structures in Orbit, Volume 1," Contract MOM7DNS-895942. GSI Technical Report 80-012, GSI, Melbourne, FL, Sept. 1980.

Earl A. Thornton
Associate Editor